

Gd₃ Triangles in a Polyoxometalate Matrix: Tuning Molecular Magnetocaloric Effects in {Gd₃₀M₈} Polyoxometalate/Cluster Hybrids Through Variation of M²⁺

Masooma Ibrahim,* Yan Peng, Eufemio Moreno-Pineda, Christopher E. Anson, Jürgen Schnack,* and Annie K. Powell*

The syntheses and structures of a family of five new Ln/3d cluster containing polyoxometalates (POMs) $\{[(\text{GeW}_9\text{O}_{34})_2\text{Ln}^{\text{III}}_3(\text{CO}_3)(\text{OH}_2)_3]_6\{3\text{M}^{\text{II}}_2\text{Ln}^{\text{III}}_3(\mu_3\text{-OH})_6(\text{OH}_2)_6\}_4\}^{50-}$ {Ln₃₀M₈}, where Ln = Gd or Y, and M = Zn, Mn, Co, are presented. This structural motif of a giant tetrahedron contains {Ln^{III}₃} and {M^{II}₂Ln^{III}₃}-cluster units which are well-isolated within the diamagnetic polyoxotungstate system. The magnetic properties of {Gd₃₀Mn₈}, {Y₃₀Mn₈} and {Gd₃₀Zn₈} can be successfully modeled using a Heisenberg approach. Investigation of their magnetocaloric effect (MCE) reveals that this can be tuned through variation of the 3d metal ion. This is the first such systematic study on heterometallic 3d-4f- POM clusters. The {Gd₃₀Zn₈} analogue illustrates a promising way forward to magnetic cooling at sub-Kelvin temperatures.

1. Introduction

In polyoxometalate (POM) chemistry a large variety of compounds can be constructed by linking together metal–oxygen building blocks.^[1–3] Among these, POM/coordination cluster (CC) hybrids are becoming increasingly well-established with examples combining POMs with various 3d and/or rare-earth ions, the majority of the latter involving diamagnetic species such as Y^{III} and La^{III}.^[4–11]

In a class of their own are the highly symmetric spherical Keplerate systems. These have received much attention not only because of their aesthetically beautiful structures but also because of their interesting

properties.^[12–18] In these compounds, the Mo centers within the POM units are present both as fully oxidized diamagnetic Mo^{VI} and 4d¹ Mo^V. The basic building block of the Keplerate is a mixed-valent {(Mo)Mo₅} pentagonal unit and when 12 of these are placed at the vertices of an icosahedron with 30 mono- or di-nuclear (L) units linking these together, compounds such as {Mo₇₂Fe₂₄Ln₆O₂₅₂} result.^[18] In this particular case, the Fe and Ln (Ce or Pr) are trivalent and delocalized over the structure. The overall charge is balanced by 54 formally diamagnetic Mo^{VI} and 18 paramagnetic Mo^V metal ions. Further systems with linkers L = Fe^{III}, Cr^{III}, V^{IV} with S = 5/2, 3/2 and 1/2, respectively, have been described.

Recently, we reported on an entirely different approach to targeting POM/CC paramagnetic hybrids with the structure and magnetic properties of $\{[(\text{GeW}_9\text{O}_{34})_2\text{Dy}^{\text{III}}_3(\mu_2\text{-OH})_3(\text{H}_2\text{O})]_6\{ \text{Co}^{\text{II}}_2\text{Dy}^{\text{III}}_3-(\mu_3\text{-OH})_6(\text{OH}_2)_6\}_4\}^{56-}$ {Dy₃₀Co₈}, which shows SMM behavior.^[19] This compound has a hollow tetrahedral cage structure with six fully oxidized, diamagnetic {(GeW^{VI}₉O₃₄)₂Dy^{III}₃} units acting as linkers (edges) and four {Dy^{III}₃Co^{II}₂} clusters as nodes (vertices) to form the giant tetrahedron. Not only is this an inverted means in comparison with the Keplerate hybrids to achieve a nanoscale superstructure, but also, in this case, the 3d and 4f metal ions are completely localized in the form of well-defined coordination clusters.

As in the case of the Keplerate POMs, the generic {Ln₃₀Co₈} polytungstate system provides a platform for variation/replacement of paramagnetic ions, but here within a fully diamagnetic POM matrix. This allows for the detailed study of the magnetic behavior of the clusters. Since the overall structural features

Dr. M. Ibrahim, Dr. E. Moreno-Pineda, Prof. A. K. Powell
Institute of Nanotechnology (INT)
Karlsruhe Institute of Technology (KIT)
Hermann-von-Helmholtz Platz 1, 76344 Eggenstein-Leopoldshafen,
Germany
E-mail: masooma.ibrahim@kit.edu; annie.powell@kit.edu

Dr. Y. Peng, Dr. C. E. Anson, Prof. A. K. Powell
Institute of Inorganic Chemistry
Karlsruhe Institute of Technology (KIT)
Engesserstrasse 15, 76131 Karlsruhe, Germany

Dr. E. Moreno-Pineda
Depto. de Química-Física
Escuela de Química
Facultad de Ciencias Naturales
Exactas y Tecnología
Universidad de Panamá
Panamá, Panamá

Prof. J. Schnack
Faculty of Physics
Bielefeld University
PF 100131, D-33501 Bielefeld, Germany
E-mail: jschnack@uni-bielefeld.de

 The ORCID identification number(s) for the author(s) of this article can be found under <https://doi.org/10.1002/ssstr.202100052>.

© 2021 The Authors. Small Structures published by Wiley-VCH GmbH. This is an open access article under the terms of the Creative Commons Attribution-NonCommercial-NoDerivs License, which permits use and distribution in any medium, provided the original work is properly cited, the use is non-commercial and no modifications or adaptations are made.

DOI: 10.1002/ssstr.202100052

remain essentially the same, the individual paramagnetic metal ion contributions to the magnetic properties can be explored. This presents the opportunity to draw conclusions regarding the interplay of magnetic and structural properties within a single overall architecture provided by the giant tetrahedral arrangement of the building blocks.

Considering the various tuning handles available, we decided to explore variations to the metal ions within this system in terms of the potential of the compounds to act as magnetic refrigerants. Among the possibilities here is employing the useful strategy of deleting magnetic contributions to the overall picture through choosing substitution of the Co^{II} with diamagnetic Zn^{II} or else Dy^{III} with diamagnetic Y^{III} as well as changing the nature of the paramagnetic ion from Co^{II} to the isotropic Mn^{II} or Dy^{III} to the isotropic Gd^{III} ion, both of which also show the maximum spin value available in their respective series.

The magnetocaloric effect (MCE) can be defined as the cooling or heating of magnetic materials when sweeping the external magnetic field. Several groups have reviewed progress in using molecules as refrigerants with an emphasis on manipulation of chemical composition for fine-tuning the magnetothermal properties.^[20] One motivation here is to produce systems providing sub-Kelvin cooling to provide an alternative to the increasingly rare and expensive ^3He cryogen.

Although all spin clusters intrinsically display the MCE, the magnitude of the effect depends on the nature of each material. Among molecular magnets, gadolinium-based clusters are the most promising magnetic coolers as the isotropic $^8S_{7/2}$ ground state of the Gd^{3+} ion provides the largest magnetic entropy per single ion. From a synthetic point of view, an effective strategy to design materials with a high MCE has proved to be the use of 3d– Gd^{III} cluster compounds.^[20–24] Evangelisti and coworkers have carried out MCE studies on the complexes $[\text{Gd}(\text{W}_5\text{O}_{18})_2]^{9-}$ and $[\text{Gd}(\text{P}_5\text{W}_{30}\text{O}_{110})]^{12-}$, in which they used the POM metallo-ligands to create systems containing magnetically isolated Gd^{III} centers that would allow cooling by MCE at very low temperatures.^[23] However, to date there have been no reported studies of MCE in 3d– Gd^{III} -containing POMs.

Thus we report here the extension of our previous work on $\{\text{Dy}_{30}\text{Co}_8\}^{[19]}$ to its Gd^{III} analogue, $\{\text{Gd}_{30}\text{Co}_8\}$ and to the isostructural $\{\text{Gd}_{30}\text{Mn}_8\}$ and $\{\text{Gd}_{30}\text{Zn}_8\}$ compounds. The last of these corresponds to weakly coupled Gd_3 triangles in a magnetically insulating POM matrix, while the other two allow us to investigate the potential for tuning MCE effects by addition of isotropic Mn^{II} or anisotropic Co^{II} cations, respectively. Further analogues containing diamagnetic Y^{III} , $\{\text{Y}_{30}\text{Mn}_8\}$ and $\{\text{Y}_{30}\text{Co}_8\}$, allow us to probe the contributions of the 3d cations alone. We have previously reported the use of the $\{\text{Gd}_{30}\text{Co}_8\}$ and $\{\text{Dy}_{30}\text{Co}_8\}$ compounds as novel MRI contrast reagents.^[25]

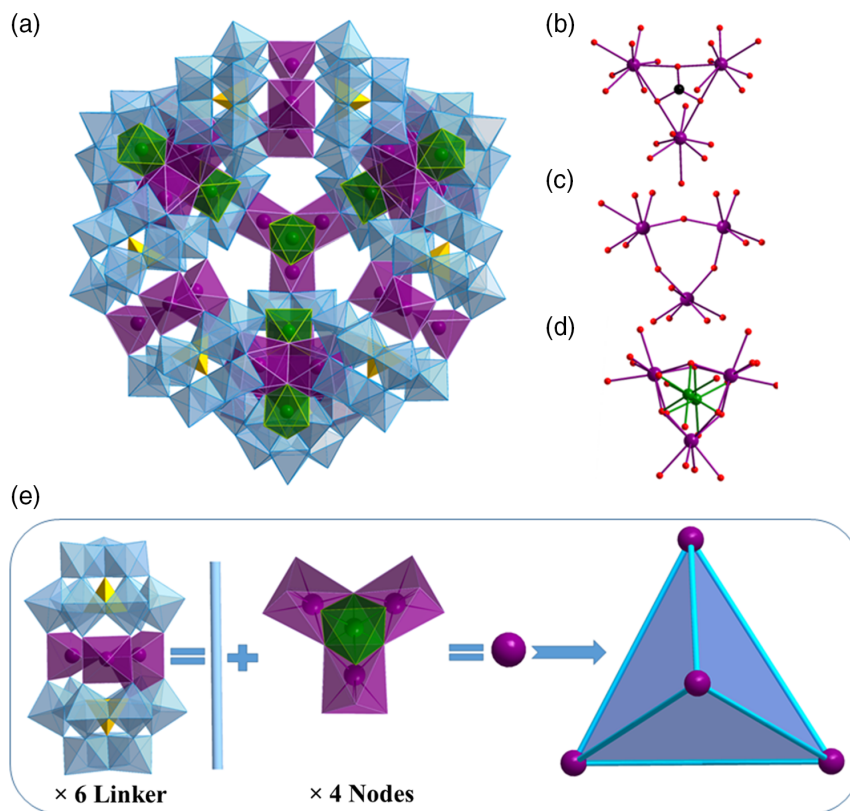


Figure 1. a) Polyhedral representation of Ln_{30}M_8 . b) $\{\text{Ln}^{\text{III}}_3(\text{CO}_3)(\text{OH}_2)\}$ core in sandwich-type building block linker $\{(\text{GeW}_9\text{O}_{34})_2\text{Ln}^{\text{III}}_3(\text{CO}_3)(\text{OH}_2)\}$. c) $\{\text{Dy}^{\text{III}}_3(\text{OH})_3(\text{OH}_2)\}$ core in sandwich-type building block linker $\{(\text{GeW}_9\text{O}_{34})_2\text{Dy}^{\text{III}}_3(\text{OH})_3(\text{OH}_2)\}$ of $\text{Dy}_{30}\text{Co}_8$. d) Heterometallic node $\{3\text{d}^{\text{II}}_2\text{Ln}^{\text{III}}_3(\mu_3\text{-OH})_6(\text{OH}_2)_6\}$. e) The building blocks of Ln_{30}M_8 . The giant tetrahedral architecture in Ln_{30}M_8 is formed by connection of the six linker $\{(\text{GeW}_9\text{O}_{34})_2\text{Ln}^{\text{III}}\}$ units via four $\{\text{Ln}^{\text{III}}_33\text{d}^{\text{II}}_2\}$ heterometallic node units. Polyhedral color scheme: WO_6 blue, GeO_4 yellow, 3dO_6 green, LnO_n violet. Color scheme for balls: Ln = violet, O = red, C = black, and 3d = green.

2. Results and Discussion

The POM clusters $\{\text{Ln}_{30}\text{M}_8\}$ ($\text{Ln} = \text{Gd}^{\text{III}}, \text{Y}^{\text{III}}, \text{M} = \text{Co}^{\text{II}}, \text{Mn}^{\text{II}}, \text{Zn}^{\text{II}}$) were isolated from aqueous basic solution containing a mixture of appropriate 3d and Ln salts plus $[\text{GeW}_9\text{O}_{34}]^{10-}$. This one-pot self-assembly synthetic strategy has proved to be a successful approach to prepare structurally diverse and oligomeric POM structures. The overall giant-tetrahedral architecture of these nanocluster $\{\text{Ln}_{30}\text{M}_8\}$ molecules is essentially the same as for our previously reported $\{\text{Dy}_{30}\text{Co}_8\}$ analogue.^[9] Indeed, $\{\text{Gd}_{30}\text{Co}_8\}$, $\text{Cs}_{20}\text{Co}^{\text{II}}_6\text{Na}_{42}\{[(\text{GeW}_9\text{O}_{34})_2\text{Gd}^{\text{III}}_3(\mu\text{-OH})_3(\text{OH}_2)_3]_6\} \{\text{Co}^{\text{II}}_2\text{Gd}^{\text{III}}_3(\mu_3\text{-OH})_6(\text{OH}_2)_6\}_4\} \cdot 340\text{H}_2\text{O}$, crystallizes isomorphously to $\{\text{Dy}_{30}\text{Co}_8\}$ in $P\bar{3}$ with $Z = 2$, and, apart from the change of lanthanide, only differs in the mix of counteranions. The edges of the giant tetrahedron are thus provided by six $\{(\text{GeW}_9\text{O}_{34})_2\text{Gd}^{\text{III}}_3(\mu\text{-OH})_3(\text{OH}_2)_3\}$ linkers and its vertices by four heterometallic $\{\text{Co}^{\text{II}}_2\text{Gd}^{\text{III}}_3(\mu\text{-OH})_6(\text{OH}_2)_6\}$ nodes (Figure 1a,e).

The compounds $\text{CsMn}^{\text{II}}_6\text{Na}_{37}\{[(\text{GeW}_9\text{O}_{34})_2\text{Gd}^{\text{III}}_3(\text{CO}_3)(\text{OH}_2)_6\} \{\text{Mn}^{\text{II}}_2\text{Gd}^{\text{III}}_3(\mu_3\text{-OH})_6(\text{OH}_2)_6\}_4\} \cdot 295\text{H}_2\text{O}$ $\{\text{Gd}_{30}\text{Mn}_8\}$, $\text{CsZn}_2\text{Na}_{45}\{[(\text{GeW}_9\text{O}_{34})_2\text{Gd}^{\text{III}}_3(\text{CO}_3)(\text{OH}_2)_6\} \{\text{Zn}_2\text{Gd}^{\text{III}}_3(\mu_3\text{-OH})_6(\text{OH}_2)_6\}_4\} \cdot 295\text{H}_2\text{O}$ $\{\text{Gd}_{30}\text{Zn}_8\}$ and $\text{Cs}_{10}\text{Co}^{\text{II}}_6\text{Na}_{28}\{[(\text{GeW}_9\text{O}_{34})_2\text{Y}^{\text{III}}_3(\text{CO}_3)(\text{OH}_2)_3]_6\} \{\text{Co}^{\text{II}}_2\text{Y}^{\text{III}}_3(\mu_3\text{-OH})_6(\text{OH}_2)_6\}_4\} \cdot 350\text{H}_2\text{O}$ $\{\text{Y}_{30}\text{Co}_8\}$ form a separate isomorphous series, crystallizing in $C2/c$ with $Z = 4$. A slight structural difference compared to the previous two compounds is that the Ln_3 triangles “sandwiched” at the centers of the linker moieties are now bridged by one $(\mu_3\text{-CO}_3)^{2-}$ ligand

instead of the three hydroxo-bridges. Such carbonate bridges are similar to those reported in a family of POMs formulated as $[(\text{XW}_9\text{O}_{34})_2\text{Ln}^{\text{III}}_3(\mu_3\text{-CO}_3)(\text{OH}_2)_3]^{n-}$,^[26,27] which correspond to the linkers in the structures reported here. Finally, $\text{Cs}_{0.5}\text{Y}_{3.5}\text{Mn}_6\text{Na}_{31}\{[(\text{GeW}_9\text{O}_{34})_2\text{Y}^{\text{III}}_3(\text{CO}_3)(\text{OH}_2)_3]_6\} \{(\text{GeW}_9\text{O}_{34})_2\text{Y}^{\text{III}}_3(\text{CO}_3)(\text{OH}_2)_3\}_4\} \{\text{Mn}^{\text{II}}_2\text{Y}^{\text{III}}_3(\mu_3\text{-OH})_6(\text{OH}_2)_6\}_4\} \cdot 310\text{H}_2\text{O}$ $\{\text{Y}_{30}\text{Mn}_8\}$ crystallizes in $P4_2/nmc$ with $Z = 2$, and here the Y_3 triangles within the linkers are disordered in the structure. On average four such Y_3 triangles per giant tetrahedron are bridged by three hydroxo ligands and two by carbonate bridges (Figure 1b,c).

The $\text{Gd}_3(\mu_3\text{-CO}_3)$ triangles sandwiched between W_9 units are essentially equilateral, and the $\text{Gd}\cdots\text{Gd}$ distances within them average 4.88 Å, while the $\text{Gd}_3(\mu\text{-OH})_3$ triangles in $\{\text{Gd}_{30}\text{Co}_8\}$ are somewhat smaller, with $\text{Gd}\cdots\text{Gd}$ averaging 4.45 Å. The $\text{Gd}\text{-O}\text{-Gd}$ geometries also differ, with $\text{Gd}\text{-O}$ averaging 2.42 Å and $\text{Gd}\text{-O}\text{-Gd}$ averaging 175.2° for the carbonate-bridged triangles, whereas the corresponding values for the hydroxide bridges in $\{\text{Gd}_{30}\text{Co}_8\}$ are 2.30 Å and 153.1°. Within the $\text{Gd}_3\text{M}_2(\mu_3\text{-OH})_6$ subclusters, the Gd_3 triangles are again equilateral, with $\text{Gd}\cdots\text{Gd}$ averaging 3.61 Å and not differing significantly with M. Similarly, the $\text{Gd}\text{-O}\text{-Gd}$ angles average 103.2° and $\text{Gd}\text{-O}$ 2.41 Å, again with no significant differences between the three Gd-containing systems. The $\text{M}\text{-}(\mu_3\text{-OH})$, as expected, do differ according to M, with $\text{Mn}\text{-O}$, $\text{Co}\text{-O}$, and $\text{Zn}\text{-O}$ averaging 2.17, 2.10, and 2.10 Å, respectively. The shortest intertriangle $\text{Gd}\cdots\text{Gd}$ distance in $\{\text{Gd}_{30}\text{Zn}_8\}$ is 6.36 Å, corresponding to one Gd in a “sandwiched” triangle and another Gd in a Gd_3Zn_2 moiety.

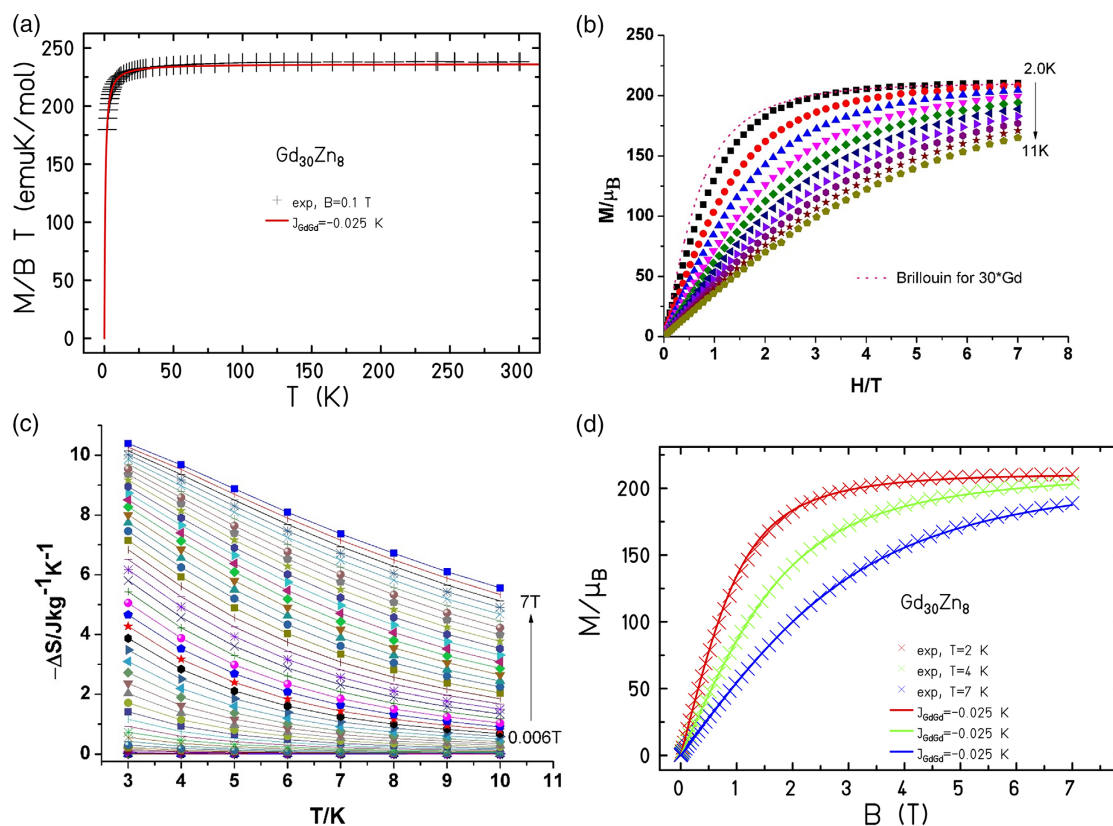


Figure 2. a) Plot of χT versus T . b) Plots of M versus H . c) Magnetic entropy changes. d) Fitting the magnetization data with ten isolated $\{\text{Gd}_3\}$ triangles model assuming the interactions within the triangle are equal for $\text{Gd}_{30}\text{Zn}_8$.

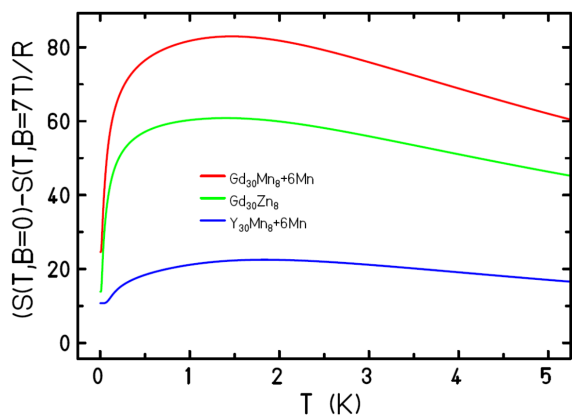


Figure 3. The calculated entropy changes for $\text{Gd}_{30}\text{Zn}_8$, Y_{30}Mn_8 and $\text{Gd}_{30}\text{Mn}_8$ with the J parameters obtained from fitting the χT versus T and M versus H plots.

It should be noted from the elemental analyses that the counterions in the structures are not just Na^+ and Cs^+ , but also include the respective 3d cations and these are included in the magnetic analyses, where they are found to be isolated magnetically.

The room temperature $\chi_M T$ value (where χ_M is the molar magnetic susceptibility) of the $\text{Gd}_{30}\text{Zn}_8$ complex is $239.4 \text{ cm}^3 \text{ K mol}^{-1}$, agreeing well with the expected value of $236.3 \text{ cm}^3 \text{ K mol}^{-1}$ for 30 noninteracting Gd^{III} ions. Upon cooling, the χT product stays

practically constant until $\approx 16 \text{ K}$, below which it decreases rapidly, reaching a χT value of $179.2 \text{ cm}^3 \text{ K mol}^{-1}$ at 2 K (Figure 2a). The molar magnetization, M , as a function of applied field (H) at 2 K , saturating for fields above 4 T at $210.7 \mu_B$ (Figure 2b) in line with the expected value for 30 Gd^{III} ions. The curve lies only just below the calculated Brillouin function for noninteracting Gd^{III} , spins indicating very weak antiferromagnetic interactions within the Gd_3 triangles.

To quantify these interactions, the χT versus T and M versus H plots were fitted using a model of ten isolated $\{\text{Gd}_3\}$ triangles with a Heisenberg spin Hamiltonian with convention $H = -2J[S_a \cdot S_b]$. To avoid over parameterization, a common coupling constant was assigned to both types of Gd_3 triangles,^[28] giving $g = 2.00$ and $J_{\text{Gd-Gd}} = -0.025 \text{ K}$ (Figure 2d). Previously, Soncini and Bosovic carried out detailed analyses of the Ln-Ln interactions in the related POM-based clusters $[(\text{XW}_9\text{O}_{34})_2\text{Ln}^{\text{III}}_3(\mu_3\text{-CO}_3)(\text{OH}_2)_3]^{11-}$ (Ln = Tb, Dy, Ho, Er) but could not obtain a Gd analogue.^[27] However, two other magnetic studies of clusters containing similar $\{\text{Gd}_3(\mu_3\text{-CO}_3)\}$ triangles have yielded $J_{\text{Gd-Gd}} = -0.006$ ^[28] and -0.030 K ,^[29] comparable with the value obtained here.

We then investigated the magnetocaloric properties of the $\text{Gd}_{30}\text{Zn}_8$ compound. The magnetic entropy changes of $\text{Gd}_{30}\text{Zn}_8$ (Figure 2) were assessed using the Maxwell equation $\Delta S = \int [\partial M(T, M) / \partial T]_H dH$. This gives a magnetic entropy change $-\Delta S = 10.4 \text{ J kg}^{-1} \text{ K}^{-1}$ for fields varying from 0 to 7 T at 3 K , which is slightly lower (81.3%) than the theoretical total

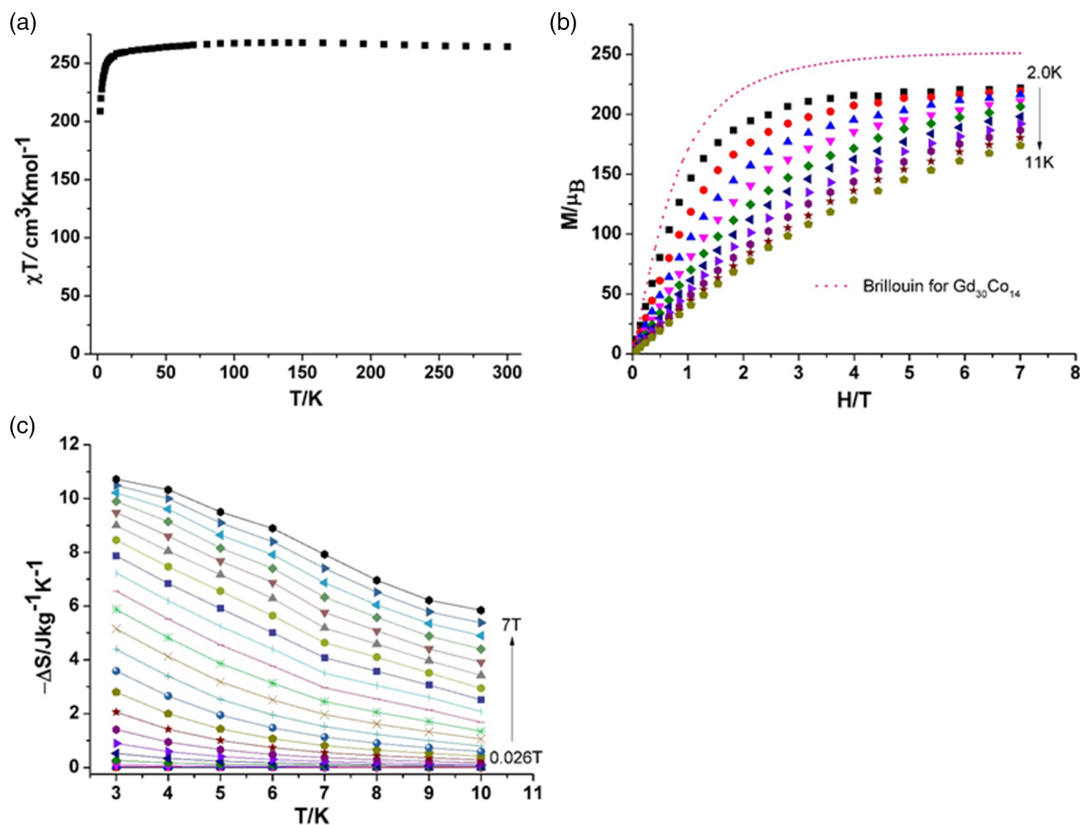


Figure 4. a) Plot of χT versus T . b) Plots of M versus H . c) Magnetic entropy changes for $\text{Gd}_{30}\text{Co}_8$.

entropy value of $12.8 \text{ J kg}^{-1} \text{ K}^{-1}$ for $\text{Gd}_{30}\text{Zn}_8$ calculated using $-\Delta S_m = (\sum n R \ln(2s_n + 1))/M_r$ (R is the gas constant) as a result of the weak antiferromagnetic coupling (Figure 3 and S6, Supporting Information). This value of $-\Delta S$ can be compared with that of $22.6 \text{ J kg}^{-1} \text{ K}^{-1}$ obtained for a Gd_6 cluster in which the cluster core is composed of fused $\text{Gd}_3(\text{CO}_3)$ triangles^[28] similar to those found here; the higher value in this case is largely accounted for by the lower formula weight per Gd^{III} . Indeed, if one calculates the entropy change per unit volume, which might well be the more relevant parameter in some applications, $-\Delta S$ for $\text{Gd}_{30}\text{Zn}_8$ is now $38.42 \text{ kJ m}^{-3} \text{ K}^{-1}$, comparable with $36.97 \text{ kJ m}^{-3} \text{ K}^{-1}$ for the carbonate-bridged Gd_6 in the study by Todea et al.,^[16] whereas the corresponding value for $\text{Gd}_{30}\text{Mn}_8$ (*vide infra*) is now significantly higher at $-\Delta S = 51.70 \text{ kJ m}^{-3} \text{ K}^{-1}$.

The room temperature χT value of the $\text{Gd}_{30}\text{Co}_8$ complex is $264.3 \text{ cm}^3 \text{ K mol}^{-1}$, which agrees well with the expected value of $263.5 \text{ cm}^3 \text{ K mol}^{-1}$ for the spin only value of 30 noninteracting Gd^{III} ($g = 2.00$ and $S = 7/2$) and 14 noninteracting Co^{II} centers (8 in the cluster, 6 as counteranions) ($g = 2.0$ and $S = 3/2$). Upon cooling, the χT product decreases relatively slowly until $\approx 15 \text{ K}$, below which it decreases more rapidly, reaching $208.87 \text{ cm}^3 \text{ K mol}^{-1}$ at 2 K (Figure 4a). The molar magnetization (M) at 2 K rises slightly more slowly than the Brillouin function, resulting in a value of $214.33 \mu_B$ at 7 T . The saturation value for 30 noninteracting Gd^{III} and 14 noninteracting Co^{II} (Figure 4b) assuming $g = 2$ is larger than the experimental

observation. This, along with the decrease in the χT product at low temperatures, suggests a degree of antiferromagnetic coupling and/or anisotropy effects.

The magnetic entropy changes of $\text{Gd}_{30}\text{Co}_8$ were also calculated (Figure 4c) and gave a value of $10.72 \text{ J kg}^{-1} \text{ K}^{-1}$ for $\Delta H = 0-7 \text{ T}$ at 3 K . The low $-\Delta S_m$ value is also in line with the presence of antiferromagnetic interactions and/or the anisotropic nature of Co^{II} in the $\text{Gd}_{30}\text{Co}_8$ complex.

Comparison of the experimental $-\Delta S_m$ with the theoretical value clearly shows that only 64.8 % (at 3 K and 7 T) of the total magnetic entropy is accessed. The room temperature χT value of the $\text{Gd}_{30}\text{Mn}_8$ complex is $300.1 \text{ cm}^3 \text{ K mol}^{-1}$, which is close to the spin only value at room temperature for 30 noninteracting Gd^{III} and 14 isolated Mn^{II} ($297.50 \text{ cm}^3 \text{ K mol}^{-1}$ for 30 Gd^{III} with $g = 2.00$ and $S = 7/2$ and 14 Mn^{II} ions [again, 8 in the cluster and 6 as counteranions], with $g = 2$ and $S = 5/2$). Upon cooling, the χT product stays practically constant until $\approx 15 \text{ K}$, below which it decreases rapidly, reaching a χT value of $259.7 \text{ cm}^3 \text{ K mol}^{-1}$ at 2 K (Figure 5a). The molar magnetization (M) at 2 K rises slightly more slowly than the corresponding Brillouin function, indicative of weak antiferromagnetic interactions, and reaches a saturation value of $285.6 \mu_B$ at 2 K and 7 T (Figure 5b). The χT versus T and M versus H (B) plots are reproduced very well by introducing equal $J_{\text{Mn-Gd}}$ values in the four Mn_2Gd_3 units, while fixing the $J_{\text{Mn-Mn}}$ to that found for Y_{30}Mn_8 ($J_{\text{Mn-Mn}} = -0.2 \text{ K}$, see Supporting Information) and the $J_{\text{Gd-Gd}}$ to that found for $\text{Gd}_{30}\text{Zn}_8$ ($J_{\text{Gd-Gd}} = -0.025 \text{ K}$). The best fit was obtained with

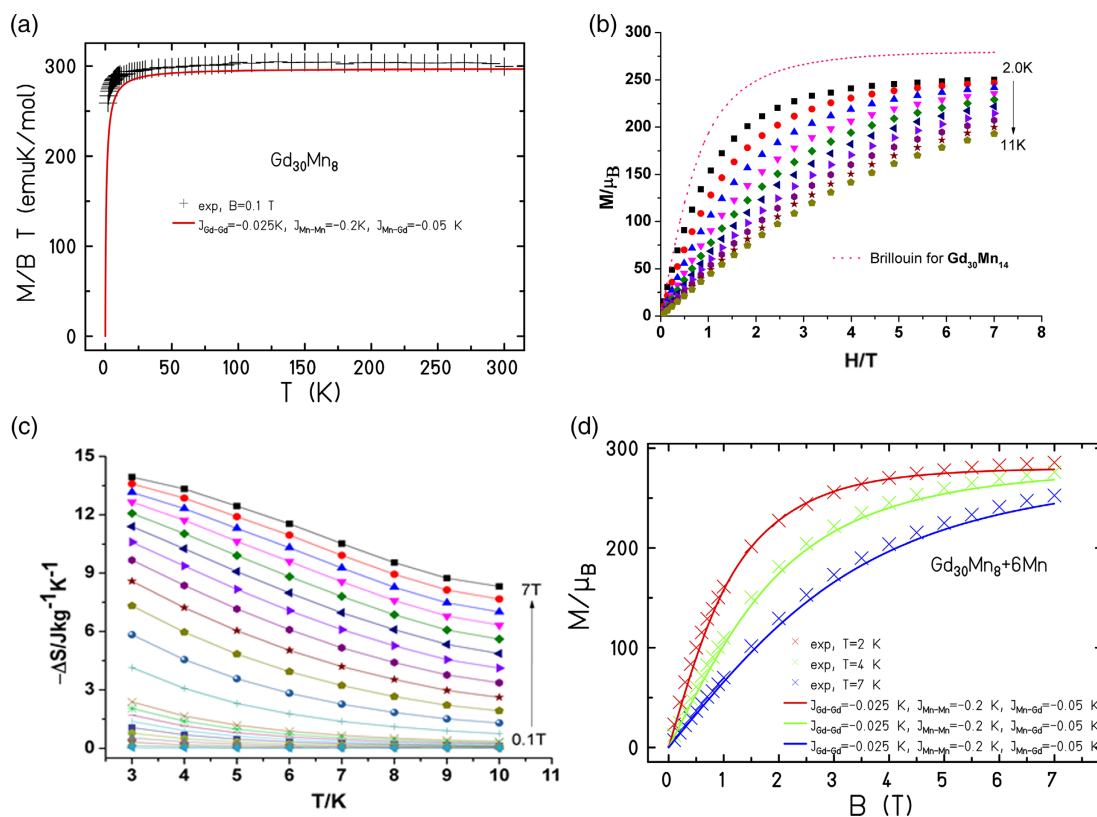


Figure 5. a) Plot of χT versus T . b) Plots of M versus H . c) Magnetic entropy changes. d) Fitting the magnetization data by introducing 18 equal $J_{\text{Mn-Gd}}$ in four isolated $\{\text{MnGd}_3\text{Mn}\}$ and fixing the $J_{\text{Mn-Mn}}$ from $\text{Gd}_{30}\text{Zn}_8$ and $J_{\text{Gd-Gd}}$ from the $\text{Gd}_{30}\text{Zn}_8$ for $\text{Gd}_{30}\text{Mn}_8$.

$J_{Mn-Gd} = -0.05$ K. The magnetic entropy change of $Gd_{30}Mn_8$ is 14.0 J $kg^{-1} K^{-1}$ for $\Delta H = 0-7$ T at 2 K (Figure 5c), which is again lower than the maximum magnetic entropy difference for non-interacting centers $87.5 R$ (18.0 J $kg^{-1} K^{-1}$) according to $-\Delta S_m = (\sum n R \ln(2s_n + 1))/M_r$. As for the $Gd_{30}Co_8$ analogue, this is most likely attributable to the antiferromagnetic exchange operating within the molecule and crystal-field effects. However, in this case, the percentage entropy change is 77.8% and thus much higher than for the $Gd_{30}Co_8$ analogue (64.8%).

It is also possible to calculate the entropy changes for $Gd_{30}Zn_8$, $Y_{30}Mn_8$, and $Gd_{30}Mn_8$ directly using the J parameters obtained from fitting the χT versus T and M versus H plots (Figure 3 and S8–S10, Supporting Information). The results for $T = 2$ K compare well to the entropy changes extracted from the experimental M versus H plots: $Gd_{30}Zn_8$, $-\Delta S = 12.2$ (exp. 10.4) J $kg^{-1} K^{-1}$, $Y_{30}Mn_8$ $-\Delta S = 4.8$ (exp 4.1) J $kg^{-1} K^{-1}$, $Gd_{30}Mn_8$ $-\Delta S = 16.8$ (exp 14.0) J $kg^{-1} K^{-1}$.

3. Conclusions

In conclusion, five discrete POM molecules with a giant tetrahedral architecture, $\{[(GeW_9O_{34})_2Ln^{III}_3(CO_3)(OH_2)_3]_6\{M^{II}_2Ln^{III}_3(\mu_3-OH)_6(OH_2)_6\}_4]^{50-} \cdot \{Ln_{30}M_8\}$ ($Ln = Gd, Y; M = Co, Mn, Zn$), containing two types of coordination clusters $\{(GeW_9O_{34})_2Ln^{III}_3\}$ as edges/linkers and $\{Ln^{III}_3M^{II}_2\}$ as vertices/nodes of a giant tetrahedron, have been synthesized and magnetically characterized. The Gd^{III} -3d POMs studied here clearly show a capability for magnetic cooling at low temperatures through their MCE. Although the entropy changes per unit weight are not particularly high in consequence of the heavy POM ligands, the values per unit volume are definitely encouraging, which would be advantageous in systems where space is of the essence. Addition of isotropic Mn^{II} to the system increased the overall ΔS , although at the cost that this was now a lower percentage of the theoretical value. In contrast, addition of anisotropic Co^{II} had a detrimental effect. Although the POM–metalloligands are heavy, they are also dense, and the ΔS values as a function of unit volume (rather than mass) indicate the potential of such compounds for magnetic cooling where space is at a premium.

It has previously been shown that complexes with single Gd^{III} centers isolated from each other by POM ligands, in which dipolar interactions have been largely suppressed and T_c greatly lowered, can be used for magnetic cooling down to ≈ 10 mK.^[23] In the $\{Gd_{30}Zn_8\}$ compound presented here, interactions between the Gd_3 triangles should similarly be quenched, leaving only the very weak antiferromagnetic intratriangle Gd – Gd interactions operative. The system may show a relatively low T_c , with the potential for significant sub-Kelvin magnetic cooling in this frustrated magnetic system.^[30] However, such dipolar interactions are notoriously hard to calculate, and further work on these compounds will clarify this intriguing possibility.

Supporting Information

Supporting Information is available from the Wiley Online Library or from the author.

Acknowledgements

M.I. and A.K.P. acknowledge support by the Helmholtz Society through the POF program Science and Technology of Nanosystems (STN). E.M.P. thanks the Panamanian National Systems of Investigators (SNI, SENACYT) for support. We thank Herman Claassen and Kaspar Uuselu for assistance in the lab. We acknowledge the Synchrotron Light Source ANKA for provision of instrumentation at the SCD beamline and Dr. Gernot Buth for assistance in measuring datasets for the crystal structures of two of the compounds, and thank Prof. Dieter Fenske and KNMF for measuring datasets for the other three compounds. The authors thank Sven Stahl and Dr. Thomas Bergfeldt for the TGA measurement and elemental analyses, respectively. The authors thank the COST Actions MultiComp (CA15107) and MOLSPIN (CA15128), and the Erasmus Mundus programme for financial support.

Open access funding enabled and organized by Projekt DEAL.

Conflict of Interest

The authors declare no conflict of interest.

Data Availability Statement

The data that supports the findings of this study are available in the supplementary material of this article.

Keywords

heterometallics, lanthanides, magnetocaloric effects, molecular magnetism, polyoxometalates, (3d/4f)

Received: April 27, 2021

Revised: June 21, 2021

Published online: July 31, 2021

- [1] A. Müller, M. Luban, C. Schröder, R. Modler, P. Kögerler, M. Axenovich, J. Schnack, P. Canfield, S. Bud'ko, N. Harrison, *ChemPhysChem* **2001**, *2*, 517.
- [2] A. V. Anyushin, A. Kondinski, T. N. Parac-Vogt, *Chem. Soc. Rev.* **2020**, *49*, 382.
- [3] M. Amiri, N. P. Martin, C. Feng, J. K. Lovio, M. Nyman, *Angew. Chem. Int. Ed.* **2021**, *60*, 12461.
- [4] J.-W. Zhao, Y.-Z. Li, L.-J. Chen, G.-Y. Yang, *Chem. Commun.* **2016**, *52*, 4418.
- [5] C. Boskovic, *Acc. Chem. Res.* **2017**, *50*, 2205.
- [6] E. Tanuhadi, E. Al-Sayed, G. Novitchi, A. Roller, G. Giester, A. Rempel, *Inorg. Chem.* **2020**, *59*, 8461.
- [7] S. Reinoso, M. Giménez-Marqués, J. R. Galán-Mascarós, P. Vitoria, J. M. Gutiérrez-Zorrilla, *Angew. Chem. Int. Ed.* **2010**, *49*, 8384.
- [8] W.-C. Chen, C.-Q. Jiao, X.-L. Wang, K.-Z. Shao, Z.-M. Su, *Inorg. Chem.* **2019**, *58*, 12895.
- [9] S.-R. Li, H.-Y. Wang, H.-F. Su, H.-J. Chen, M.-H. Du, L.-S. Long, X.-J. Kong, L.-S. Zheng, *Small Methods* **2021**, *5*, 2.
- [10] J. M. Clemente-Juan, E. Coronado, A. Gaita-Ariño, *Chem. Soc. Rev.* **2012**, *41*, 7464.
- [11] W. Wang, N. V. Izarova, J. van Leusen, P. Kögerler, *Chem. Commun.* **2020**, *56*, 14857.
- [12] A. M. Todea, A. Merca, H. Bögge, J. van Slageren, M. Dressel, L. Engelhardt, M. Luban, T. Glaser, M. Henry, A. Müller, *Angew. Chem. Int. Ed.* **2007**, *46*, 6106.
- [13] J. Schnack, *Contemp. Phys.* **2019**, *60*, 127.

- [14] A. Müller, S. Sarkar, S. Q. N. Shah, H. Bögge, M. Schmidtman, S. Sarkar, P. Kögerler, B. Hauptfleisch, A. X. Trautwein, V. Schünemann, *Angew. Chem. Int. Ed.* **1999**, *38*, 3238.
- [15] A. Müller, A. M. Todea, J. van Slageren, M. Dressel, H. Bögge, M. Schmidtman, M. Luban, L. Engelhardt, M. Rusu, *Angew. Chem. Int. Ed.* **2005**, *44*, 3857.
- [16] A. M. Todea, A. Merca, H. Bögge, T. Glaser, L. Engelhardt, R. Prozorov, M. Luban, A. Müller, *Chem. Commun.* **2009**, 3351.
- [17] B. Botar, P. Kögerler, C. L. Hill, *Chem. Commun.* **2005**, *21*, 3138.
- [18] U. Kortz, A. Müller, J. van Slageren, J. Schnack, N. S. Dalal, M. Dressel, *Coord. Chem. Rev.* **2009**, *253*, 2315.
- [19] M. Ibrahim, V. Mereacre, N. Leblanc, W. Wernsdorfer, C. E. Anson, A. K. Powell, *Angew. Chem. Int. Ed.* **2015**, *54*, 15574.
- [20] a) Y.-Z. Zheng, G.-J. Zhou, Z. Zheng, R. E. P. Winpenny, *Chem. Soc. Rev.* **2014**, *43*, 1462; b) G. Lorusso, J. W. Sharples, E. Palacios, O. Roubeau, E. K. Brechin, R. Sessoli, A. Rossin, F. Tuna, E. J. L. McInnes, D. Collison, M. Evangelisti, *Adv. Mater.* **2013**, *25*, 4653; c) M. Evangelisti, E. K. Brechin, *Dalton Trans.* **2010**, *39*, 4672; d) G. Karotsis, M. Evangelisti, S. J. Dalgarno, E. K. Brechin, *Angew. Chem. Int. Ed.* **2009**, *48*, 9928; e) M. Affronte, A. Ghirri, S. Carretta, G. Amoretti, S. Piligkos, G. A. Timco, R. E. P. Winpenny, *Appl. Phys. Lett.* **2004**, *84*, 3468.
- [21] C. Papatriantafyllopoulou, E. E. Moushi, G. Christou, A. J. Tasiopoulos, *Chem. Soc. Rev.* **2016**, *45*, 1597.
- [22] J.-B. Peng, Q.-C. Zhang, X.-J. Kong, Y.-Z. Zheng, Y.-P. Ren, L.-S. Long, R. Bin Huang, L.-S. Zheng, Z. Zheng, *J. Am. Chem. Soc.* **2012**, *134*, 3314.
- [23] M. J. Martínez-Pérez, O. Montero, M. Evangelisti, F. Luis, J. Sesé, S. Cardona-Serra, E. Coronado, *Adv. Mater.* **2012**, *24*, 4301.
- [24] X.-Y. Zheng, X.-J. Kong, Z. Zheng, L.-S. Long, L.-S. Zheng, *Acc. Chem. Res.* **2018**, *51*, 517.
- [25] M. Ibrahim, S. Krämer, N. Schork, G. Guthausen, *Dalton Trans.* **2019**, *48*, 15597.
- [26] X. Fang, T. M. Anderson, W. A. Neiwert, C. L. Hill, *Inorg. Chem.* **2003**, *42*, 8600 b) L. Yang, Q. Liu, P. Ma, J. Niu, J. Wang, *Dalton Trans.* **2015**, *44*, 13469.
- [27] M. J. Giansiracusa, M. Vonci, W. van den Heuvel, R. W. Gable, B. Moubaraki, K. S. Murray, D. Yu, R. A. Mole, A. Soncini, C. Bosovic, *Inorg. Chem.* **2016**, *55*, 5201.
- [28] S. Waqas, S. Sanz, K. S. Pedersen, M. A. Sørensen, G. S. Nichol, G. Lorusso, M. Evangelisti, E. K. Brechin, S. Piligkos, *Dalton Trans.* **2015**, *44*, 10315.
- [29] P. Bag, S. Dutta, P. Biswas, S. K. Maji, U. Flörke, K. Nag, *Dalton Trans.* **2012**, *41*, 3414.
- [30] J. W. Sharples, D. Collison, E. J. L. McInnes, J. Schnack, E. Palacios, M. Evangelisti, *Nat. Comm.*, **2014**, *5*, 5321.